

Thermal conductivity of ceramics in the $\text{ZrO}_2\text{-GdO}_{1.5}$ system

Jie Wu and Nitin P. Padture^{a)}

Department of Metallurgy and Materials Engineering, Institute of Materials Science, University of Connecticut, Storrs, Connecticut 06269-3136

Paul G. Klemens

Department of Physics, Institute of Materials Science, University of Connecticut, Storrs, Connecticut 06269-3136

Maurice Gell

Department of Metallurgy and Materials Engineering, Institute of Materials Science, University of Connecticut, Storrs, Connecticut 06269-3136

Eugenio Garca, Pilar Miranzo, and Maria I. Osendi

Instituto de Ceramica y Vidrio, CSIC, Cantoblanco, 28049 Madrid, Spain

(Received 27 August 2002; accepted 25 September 2002)

Low thermal conductivity ceramics in the $\text{ZrO}_2\text{-GdO}_{1.5}$ system have potential in structural (refractories, thermal barrier coatings, thermal protection) and nuclear applications. To that end, the thermal conductivities of hot-pressed $x\text{GdO}_{1.5} \cdot (1-x)\text{ZrO}_2$ (where $x = 0.05, 0.15, 0.31, 0.50, 0.62, 0.75, 0.89,$ and 1.00) solid solutions were measured, for the first time, as a function of temperature in the range 25 to 700 °C. On the ZrO_2 -rich side, the thermal conductivity first decreased rapidly with increasing concentration of $\text{GdO}_{1.5}$ and then reached a plateau. On the $\text{GdO}_{1.5}$ -rich side, the decrease in the thermal conductivity with increasing concentration of ZrO_2 was less pronounced. The thermal conductivity was less sensitive to the composition with increasing temperature. The thermal conductivity of pyrochlore $\text{Gd}_2\text{Zr}_2\text{O}_7$ ($x = 0.5$) was higher than that of surrounding compositions at all temperatures. A semiempirical phonon-scattering theory was used to analyze the experimental thermal conductivity data. In the case of pure ZrO_2 and $\text{GdO}_{1.5}$, the dependence of the thermal conductivity to the absolute temperature (T) was less than $1/T$. Therefore, the minimum thermal conductivity theory was applied, which better described the temperature dependence of the thermal conductivity of pure ZrO_2 and $\text{GdO}_{1.5}$. In the case of solid solutions, phonon scattering by cation mass fluctuations and additional scattering by oxygen vacancies on the ZrO_2 -rich side and by gadolinium vacancies on the $\text{GdO}_{1.5}$ -rich side seemed to account for the composition and temperature dependence of the thermal conductivity.

I. INTRODUCTION

There is a growing demand for high-temperature structural ceramics with low thermal conductivities for a variety of thermal-insulation applications. These applications include nuclear reactor components,¹ furnace walls, crucible linings, thermal barrier coatings (TBCs),² and thermal insulators. Rare-earth zirconates, which have one of the lowest thermal conductivities of all ceramics, are being explored for use in the above applications. Rare-earth zirconates, with a general formula $\text{M}_2\text{Zr}_2\text{O}_7$ ($\text{M} =$ rare earth), crystallize in the ordered pyrochlore

structure over a narrow composition range.^{3,4} At elevated temperatures the disordered fluorite is the stable phase, as it is also outside that composition range.^{3,4}

Vaßen *et al.*⁵ have measured the thermal conductivity of hot-pressed, monolithic $\text{La}_2\text{Zr}_2\text{O}_7$ ceramics (approximately 97% dense, pyrochlore phase) to be approximately $1.6 \text{ W m}^{-1} \text{ K}^{-1}$ at 700 °C, while Maloney^{6,7} has reported a thermal conductivity of approximately $1.3 \text{ W m}^{-1} \text{ K}^{-1}$ (at 700 °C) for a monolithic $\text{Gd}_2\text{Zr}_2\text{O}_7$ (fluorite phase) of unknown density. Suresh *et al.*^{1,8} have measured the thermal conductivities of porous (87 to 91% dense) materials and report values of approximately $1.5 \text{ W m}^{-1} \text{ K}^{-1}$ (at 700 °C) for $\text{M}_2\text{Zr}_2\text{O}_7$ (pyrochlore phase), which are virtually independent of the nature of the cation M ($\text{M} = \text{Eu, Gd, La, and Sm}$). Wu *et al.*⁹

^{a)}Address all correspondence to this author.
e-mail: nitin.padture@uconn.edu

have also measured thermal conductivities of fully dense $\text{M}_2\text{Zr}_2\text{O}_7$ ($\text{M} = \text{Gd}, \text{Sm}, \text{and Nd}$) to be approximately $1.6 \text{ W m}^{-1} \text{ K}^{-1}$ (at $700 \text{ }^\circ\text{C}$) and found them to be independent of the nature of the phase (pyrochlore or fluorite).

Although thermal conductivity of stoichiometric $\text{Gd}_2\text{Zr}_2\text{O}_7$ —one of the most promising low thermal conductivity candidate oxides—has been measured, there is a paucity of thermal conductivity data for solid-solutions in the system $\text{ZrO}_2\text{-GdO}_{1.5}$ in the full compositional range. Furthermore, there is a need for an adequate theory that describes the high-temperature thermal conductivity of ceramics in this and similar systems.

Thus, the objective of this work was to measure the thermal conductivities of ceramics in the $\text{ZrO}_2\text{-GdO}_{1.5}$ system, as a function of temperature and composition and to analyze them in terms of a phonon-scattering theory.

II. EXPERIMENTAL

A. Powder synthesis and specimen preparation

Ceramic powders of compositions $x\text{GdO}_{1.5} \cdot (1-x)\text{ZrO}_2$ (where $x = 0.05, 0.15, 0.31, 0.50, 0.62, 0.75,$ and 0.89) were prepared using the coprecipitation method.¹⁰ The starting materials used were $\text{Gd}(\text{NO}_3)_3 \cdot 6\text{H}_2\text{O}$ and $\text{ZrOCl}_2 \cdot 8\text{H}_2\text{O}$ (99.9% pure, Alfa Aesar, Ward Hill, MA). Individual solutions were mixed in appropriate proportions and were stirred for 30 min. The precursor solutions were slowly added to ammonia solutions (NH_3OH ; $\text{pH} = 12.5$) while being stirred to obtain gel-like precipitates, which were then filtered out and washed with distilled water. The washed precipitates were dried at $120 \text{ }^\circ\text{C}$ for 12 h and were heat treated at $500 \text{ }^\circ\text{C}$ for 10 h to remove any organics. The resulting powders were then calcined at $1500 \text{ }^\circ\text{C}$ for 24 h. The pure Gd_2O_3 powder ($x = 1.0$) was obtained from a commercial source (99.9% pure, Alfa Aesar, Ward Hill, MA). Individual powder batches were then placed in BN-coated graphite dies (25-mm diameter) and were consolidated in a hot-press (OxyGon, Nashua, NH) at a pressure of 50 MPa in flowing Ar for 0.5 h at $1500 \text{ }^\circ\text{C}$. A heating and cooling rate of $900 \text{ }^\circ\text{C h}^{-1}$ was maintained in all hot-pressing runs. The hot-pressed pellets were then annealed in air at $1500 \text{ }^\circ\text{C}$ for 12 h to oxidize the specimens completely. Since theoretical densities of the solid solutions in the $\text{ZrO}_2\text{-GdO}_{1.5}$ system are not available in the literature, the degree of densification in the hot-pressed specimens was estimated using quantitative image analysis of optical micrographs of polished cross sections. The relative density of the hot-pressed specimens was found to range between 87 to 98%.

B. Thermal conductivity measurements

Thermal-conductivity specimens of dimensions $8.7 \times 8.7 \times 1.0 \text{ mm}$ were machined out of the hot-pressed pellets. The thermal diffusivity (κ) for each material was

measured using the laser-flash method¹¹ (Thermaflash 2200, Holometrix, Bedford, MA) as a function of specimen temperature (in the range 25 to $700 \text{ }^\circ\text{C}$) in Ar atmosphere. Prior to thermal diffusivity measurements, the front and the back faces of each specimen were coated with two thin layers of gold and carbon, respectively. This was done to prevent direct transmission of the laser beam through the translucent specimens. Appropriate corrections were made in the thermal diffusivity calculations to account for the presence of these layers. The precision of the thermal diffusivity measurements is within $\pm 5\%$. The specific heat capacities (c) as a function of temperature were determined from the chemical compositions and the heat-capacity data of the constituent oxides (ZrO_2 and Gd_2O_3) obtained from the literature,¹² in conjunction with the Neumann–Kopp rule.¹³ To verify the accuracy of this method, the specific heat capacity of $\text{Gd}_2\text{Zr}_2\text{O}_7$ was measured using differential scanning calorimetry (DSC-2, Perkins Elmer, Wilmington, DE), which was found to be within $\pm 3\%$ of the calculated values in the temperature range 25 to $700 \text{ }^\circ\text{C}$. The thermal conductivity (k') for each material was then calculated using the relation $k' = \kappa\rho c$. Since some of the hot-pressed specimens were not fully dense, the resulting thermal conductivity values were normalized, to represent values for 100% dense materials (k) for ready comparison, using a previously calibrated relation:^{14,15} $k'/k = 1 - 4/3\phi$, where ϕ is the fractional porosity.

III. RESULTS

The experimental thermal conductivity data for pure ZrO_2 and $\text{GdO}_{1.5}$ are given in Figs. 1(a) and 1(b), respectively. The ZrO_2 data are taken from Raghavan *et al.*,^{16,17} while the data for $\text{GdO}_{1.5}$ are from this work. The thermal conductivity of ZrO_2 is significantly higher than that of $\text{GdO}_{1.5}$ at lower temperatures, while the conductivities for both ceramics decrease with temperature.

Figures 2(a)–2(e) show experimental thermal conductivities of ceramics in the $x\text{GdO}_{1.5} \cdot (1-x)\text{ZrO}_2$ system as a function of x , at $T = 25, 100, 300, 500,$ and $700 \text{ }^\circ\text{C}$. The following general trends in these data are observed: (i) On the ZrO_2 -rich side, the thermal conductivity decreases rapidly with increasing x and then reaches a plateau. (ii) On the $\text{GdO}_{1.5}$ -rich side, that trend is less pronounced (with decreasing x). (iii) The thermal conductivity of the solid solutions becomes less sensitive to the composition with increasing temperature. (iv) The thermal conductivity at $x = 0.5$ (pyrochlore $\text{Gd}_2\text{Zr}_2\text{O}_7$) is higher than the plateau values at all temperatures. (v) The thermal conductivity at $x = 0.89$ is higher than the trend at all temperatures.

The curves in Figs. 1 and 2 are from theoretical calculations, as described in Sec. IV.

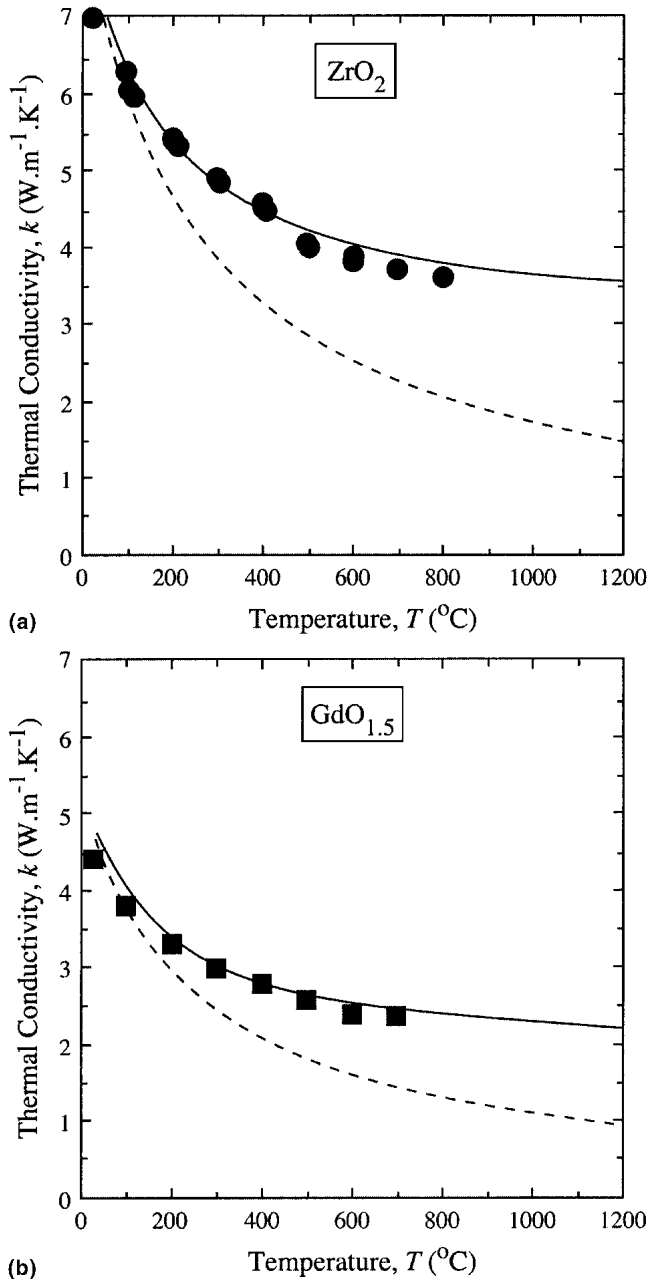


FIG. 1. Experimentally measured thermal conductivity (solid symbols), as a function of temperature, of fully dense (a) pure ZrO₂ (data from Raghavan *et al.*)^{16,17} and (b) pure GdO_{1.5}. Dashed curves represent 1/T temperature dependence [Eq. (3)], and the solid curves represent results from the minimum thermal conductivity theory [Eq. (5)].

IV. THEORY

A. Intrinsic thermal conductivities of pure ZrO₂ and GdO_{1.5}

The intrinsic mean free path of acoustic-mode phonons (limited by phonon-phonon anharmonic interactions) has been calculated to be^{18,19}

$$l_i(T, \omega) = \frac{\mu a^3 \nu \omega_D}{2\gamma^2 k_B T \omega^2 N^{1/3}} \quad (1)$$

The intrinsic thermal conductivity, using the classical specific heat of the acoustic branch, which has an upper frequency limit $\omega_D N^{-1/3}$, becomes^{18,19}

$$k_i = \left(\frac{3\chi}{2\gamma^2} \right) \left(\frac{\mu \nu^2}{N^{2/3} \omega_D} \right) T^{-1} \quad (2)$$

where ω is the phonon frequency (rad s⁻¹), k_B is the Boltzmann constant, and γ^2 is the Grüneisen anharmonicity parameter, which is taken to be equal to 4.0 for both ZrO₂ for GdO_{1.5}. There is uncertainty in the γ^2 value; however, for most oxides it is between 3.0 and 4.0.²⁰ The parameter χ is adjustable, and it is included to obtain an empirical fit between the theory and experiment at room temperature (298 K). The shear modulus represented by μ is 100 GPa for ZrO₂²¹ and 45 GPa for GdO_{1.5}.²² The transverse phonon velocity ν is given by $(\mu/\rho)^{1/2}$, where ρ is the density which is equal to 5.83 and 8.35 Mg m⁻³ for ZrO₂ and GdO_{1.5}, respectively. The velocities for ZrO₂ and GdO_{1.5} are calculated to be 4.1×10^3 and 2.3×10^3 m s⁻¹, respectively. The number of atoms per molecular unit is represented by N and is equal to 3.0 for ZrO₂ and 2.5 for GdO_{1.5}. The Debye frequency for monoatomic lattice, ω_D , is given by $(6\pi^2 \nu^3/a^3)^{1/3}$; the atomic volume a^3 is given by M_A/ρ , where M_A is the average atomic mass or mol wt/ $N_0 N$ (N_0 is the Avagadro number).¹⁹ M_A for ZrO₂ and GdO_{1.5} are 6.8×10^{-23} and 1.2×10^{-22} g, respectively. Thus, a^3 values for ZrO₂ and GdO_{1.5} are 1.2×10^{-29} and 1.4×10^{-29} m³, respectively. The Debye frequency ω_D for ZrO₂ is calculated to be 7.1×10^{13} s⁻¹, and that for GdO_{1.5} is 4.2×10^{13} s⁻¹. Thus, the temperature dependence of intrinsic thermal conductivity is given by

$$k_i = BT^{-1} \quad (3)$$

where $B = 2.2 \times 10^3$ W m⁻¹ for ZrO₂ ($\chi = 0.51$) and $B = 1.4 \times 10^3$ W m⁻¹ for GdO_{1.5} ($\chi = 0.84$). Equation (2) for ZrO₂ and GdO_{1.5} is plotted as dashed curves in Figs. 1(a) and 1(b), respectively. Figure 1 shows that the theory underestimates the experimentally measured thermal conductivities in both cases and that the deviation increases with increasing temperature. In other words, at elevated temperatures, the heat conduction provided by phonons does not vary inversely with the absolute temperature T but gradually approaches a lower limit,²⁰ as described by Roufosse and Klemens.²³

To reconcile these differences, we invoke the idea of minimum intrinsic conductivity, where the dimension of the unit cell limits the phonon mean free path (l_0), resulting in a lower limit in the thermal conductivity.²³

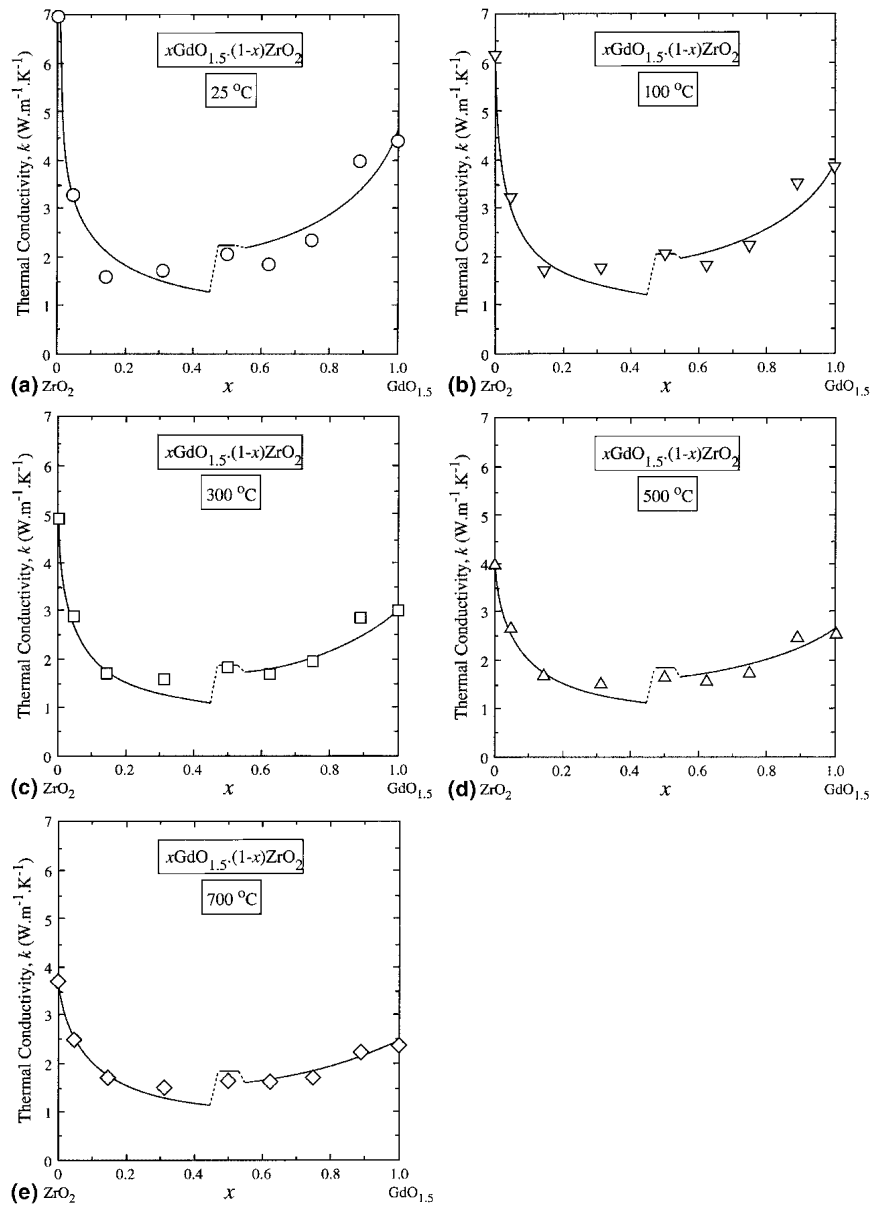


FIG. 2. Experimental thermal conductivity (open symbols) of fully dense $x\text{GdO}_{1.5} \cdot (1-x)\text{ZrO}_2$ ceramics as a function of x at (a) 25 °C, (b) 100 °C, (c) 300 °C, (d) 500 °C, and (e) 700 °C. Solid curves on the left ($0 < x < 0.5$) and on the right ($0.5 < x < 1.0$) are calculated theoretically using a combination of Eqs. (9), (10), and (12) and Eqs. (9), (10), and (20), respectively. Horizontal lines at $x = 0.5$ were calculated using a combination of Eqs. (9), (10), and (17). Dashed lines are used to connect the curves and have no theoretical significance.

Here, a critical temperature $T = T_0$ is defined where the mean free path at $\omega = \omega_D N^{-1/3}$ reaches a lower limit l_0 given by²³

$$l_0 = \frac{a^3 BN}{3\nu T_0 k_B} \quad (4)$$

Thus, at temperatures $T > T_0$, the intrinsic thermal conductivity departs from Eq. (3) and becomes²³

$$k_{i(\text{Min})} = B \left[\frac{2}{3} \left(\frac{T_0}{T} \right)^{1/2} + \frac{1}{3} \left(\frac{T_0}{T} \right) \right] T^{-1} \quad (5)$$

Fitting this expression to the measured values in Figs. 1(a) and 1(b), we obtain $T_0 = 231$ K for ZrO_2 and $T_0 = 235$ K for $\text{GdO}_{1.5}$. Equation (5) for ZrO_2 and $\text{GdO}_{1.5}$ is plotted as solid curves in Figs. 1(a) and 1(b), respectively, which better describe the trend in the experimental data.

B. Thermal conductivities of solid solutions

The thermal conductivity can be reduced by the introduction of phonon-scattering lattice imperfections. In the case of solid solutions, these are point defects: (i) substitutional atoms, (ii) vacancies, and/or (iii) interstitial

atoms. Point defect scattering is a strong function of the phonon frequency and increases rapidly with increasing frequency. If the point defects are randomly distributed, they contribute to the reciprocal of the phonon mean free path as follows^{18,19}

$$\frac{1}{l(\omega)} = \frac{1}{l_i(T, \omega)} + A\omega^4 \quad (6)$$

For simple substitutional solute of concentration c and differing in mass from the host atom of mass M by ΔM , A is given by

$$A = \frac{a^3}{4\pi v^2} c \left(\frac{\Delta M}{M} \right)^2 \quad (7)$$

The thermal conductivity in the presence of point defects then becomes^{18,19}

$$k_p = k_i \left(\frac{\omega_0}{\omega_M} \right) \tan^{-1} \left(\frac{\omega_M}{\omega_0} \right) \quad (8)$$

where ω_0 is the phonon frequency at which the mean free paths due to point-defect scattering and intrinsic scattering are equal and ω_M is the phonon frequency corresponding to the maximum of the acoustic branch of the phonon spectrum ($= \omega_D N^{-1/3}$). Since Eq. (5) describes the intrinsic thermal conductivity more accurately than Eq. (2), we replace k_i in Eq. (8) by $k_{i(\text{Min})}$:

$$k_p = k_{i(\text{Min})} \left(\frac{\omega_0}{\omega_M} \right) \tan^{-1} \left(\frac{\omega_M}{\omega_0} \right) \quad (9)$$

and

$$\left(\frac{\omega_0}{\omega_M} \right) = f \left(\frac{4\psi\gamma^2 N K_B}{3\pi\mu a^3} \right) T \left[c \left(\frac{\Delta M}{M} \right)^2 \right]^{-1} \quad (10)$$

The function f in Eq. (10) would assume a value of unity in the case of Eq. (8). However, when k_i is replaced by $k_{i(\text{Min})}$ in the case of Eq. (10), the function f is empirically defined as

$$f(T) = \frac{298 k_{i(\text{Min})} |^{298}}{T k_{i(\text{Min})} |^T} \quad (11)$$

This correction takes approximate account of the minimum mean free path as well as point defect scattering. The parameter ψ is adjustable, and it is included to obtain an empirical fit between the theory and experiment at room temperature (298 K).

To define an effective $c(\Delta M/M)^2$ parameter in Eq. (10) for different types of point defects, the solid solutions in the system $x\text{GdO}_{1.5} \cdot (1-x)\text{ZrO}_2$ are conveniently divided into three composition ranges: (i) ZrO₂-rich ($0 < x < 0.5$); (ii) pyrochlore Gd₂Zr₂O₇ ($x = 0.5$); (iii) GdO_{1.5}-rich ($0.5 < x < 1.0$).

1. ZrO₂-Rich ($0 < x < 0.5$)

The addition of GdO_{1.5} dopant to ZrO₂ creates two types of phonon-scattering point defects: (i) substitutional solute atoms (Gd on Zr sites); (ii) corresponding oxygen vacancies due to the aliovalent nature of the dopant. The scattering strength due to the disorder in the cation sites is proportional to the square of the atomic weight difference between the solute (Gd) and the host (Zr) cations. The scattering strength of oxygen vacancies is larger than substitutional solutes and is due to the missing oxygen mass and the missing interatomic bonds at the vacancy site. Thus, the term $c(\Delta M/M)^2$ is composed of two parts corresponding to the two types of point defects present, solute atoms and oxygen vacancies:

$$c \left(\frac{\Delta M}{\bar{M}} \right)^2 = x \left(\frac{\Delta M}{\bar{M}} \right)_{\text{Gd-Solute}}^2 + \frac{x}{2} \left(\frac{\Delta M_{\text{O-Vac}}}{\bar{M}} \right)_{\text{O-Vacancies}}^2 \quad (12)$$

where \bar{M} is the average atomic weight in a unit cell:

$$\bar{M} = \frac{\bar{M}_{\text{Cation}} + (2 - 0.5x)M_{\text{O}}}{3 - 0.5x} \quad (13)$$

\bar{M}_{Cation} is the average cation atomic weight:

$$\bar{M}_{\text{Cation}} = xM_{\text{Gd}} + (1-x)M_{\text{Zr}} \quad (14)$$

Also, since Gd is much heavier than Zr, it moves in opposition to the surrounding lattice, and the effective value of $(\Delta M/\bar{M})_{\text{Gd-Solute}}$ is²⁴

$$\left(\frac{\Delta M}{\bar{M}} \right)_{\text{Gd-Solute}} = \left(\frac{1}{M_{\text{Gd}}} - \frac{1}{M_{\text{Zr}}} \right) \left(\frac{1}{\bar{M}} \right)^{-1} \quad (15)$$

For oxygen vacancy:²⁵

$$\Delta M_{\text{O-Vacancies}} = (-\bar{M} \times 2) - M_{\text{O}} \quad (16)$$

where, the factor 2 in Eq. (16) arises because the number of broken bonds at the vacancy is twice the number of bonds per atom. M_{Zr} , M_{Gd} , and M_{O} are the respective atomic weights.

Equation (9) for $0 < x < 0.5$ is plotted as solid lines in Figs. 2(a)–2(e) at temperatures ranging from 25 to 700 °C ($\psi = 1.06$). The theory describes the trends in the experimental thermal conductivity data, including the dramatic decrease in the low-temperature thermal conductivity with increasing x at small values of x and the small change of the thermal conductivity at higher temperatures.

2. Pyrochlore Gd₂Zr₂O₇ ($x = 0.5$)

The compound Gd₂Zr₂O₇ exists as a disordered fluorite phase at high temperatures, and it has an ordered pyrochlore crystal structure at lower temperatures, where the cations and the oxygen vacancies are ordered.⁴ Thus,

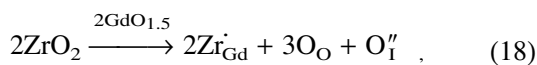
a perfect pyrochlore Gd₂Zr₂O₇ will not contain appreciable concentration of point defects. However, the relative temperature independence of the thermal conductivity of Gd₂Zr₂O₇⁹ (Fig. 2) clearly indicates the presence of some point defects. Although the calcination and hot-pressing experiments were carried out at 1500 °C, which is below the order–disorder phase transformation temperature of 1550 °C,²⁶ the resulting specimens are likely to contain both fluorite and pyrochlore phases (verified by x-ray diffraction⁹) due to the sluggish nature of that reaction. Also, during the heat treatment, the oxygen sublattice is more likely to attain its ordered structure before the cation sublattice due to faster oxygen-vacancy assisted diffusion. Thus, the point defects in the Gd₂Zr₂O₇ specimens investigated here consist mainly of random cation solute atoms. Thus, omitting the second term in Eq. (12) for the case $x = 0.5$ and from Eq. (15) we have

$$c\left(\frac{\Delta M}{\bar{M}}\right)^2 = x\left(\frac{1}{M_{\text{Gd}}} - \frac{1}{M_{\text{Zr}}}\right)^2\left(\frac{1}{\bar{M}}\right)^{-2} \quad (17)$$

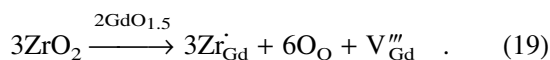
With substitution of Eq. (17) in Eq. (10), the thermal conductivity of Gd₂Zr₂O₇ is calculated using Eq. (7) and is plotted as horizontal solid lines in Figs. 2(a)–2(e) at temperatures ranging from 25 to 700 °C. Once again, the calculated values capture the trend in the measured thermal conductivity of Gd₂Zr₂O₇. The pyrochlore phase exists over a range of composition near $x = 0.5$; the thermal conductivity variation as a function of composition within the pyrochlore phase was not investigated.

3. GdO_{1.5}-Rich (0.5 < x < 1.0)

On the GdO_{1.5}-rich side, ZrO₂ is the dopant, resulting in the following possible point-defect reactions, written in the Kröger–Vink notation



and



Since the ionic size of O is large, the formation of O interstitials is not expected. Therefore, the formation of Gd vacancies and reaction given by Eq. (19) will be favored. Thus, for the GdO_{1.5}-rich case, the relation analogous to Eq. (12) becomes

$$c\left(\frac{\Delta M}{\bar{M}}\right)^2 = (1-x)\left(\frac{\Delta M}{\bar{M}}\right)_{\text{Zr-Solute}}^2 + \frac{(1-x)}{3}\left(\frac{\Delta M_{\text{GdVac}}}{\bar{M}}\right)_{\text{Gd-Vacancies}}^2 \quad (20)$$

where in the second term

$$\Delta M_{\text{GdVac}} = -M_{\text{Gd}} \quad (21)$$

There are two extreme cases of phonon scattering by vacancies: scattering due to the missing atomic mass [Eq. (21)] and scattering due to the missing atomic mass and the missing bonds [Eq. (18)].²⁷ The difference arises from the electronic state of the vacancy. It appears from our data that the anion vacancy follows the first model [Eq. (18)] and the cation vacancy follows the second [Eq. (21)]. Since Zr is lighter and follows the motion of the surrounding Gd-rich lattice, in the first term of Eq. (20)

$$\Delta M = M_{\text{Zr}} - M_{\text{Gd}} \quad (22)$$

With substitution of Eq. (20) into Eq. (10) and using appropriate values for the constants for GdO_{1.5} in Eq. (10), the resulting Eq. (9) for 0.5 < x < 1.0 is plotted as solid lines in Figs. 2(a)–2(e) at temperatures ranging from 25 to 700 °C ($\psi = 2.95$). Once again, on the GdO_{1.5}-rich side, the theory describes well the trends in the experimental thermal conductivity data.

The results of all these theoretical calculations are summarized in Fig. 3 as a function of composition at fixed temperatures.

V. DISCUSSION

We have measured the thermal conductivity of ceramics in the ZrO₂-GdO_{1.5} system as a function of composition and temperature. A semiempirical model was successfully applied to describe the effects of composition and temperature on the thermal conductivity of these ceramics. First consider the thermal conductivity of pure

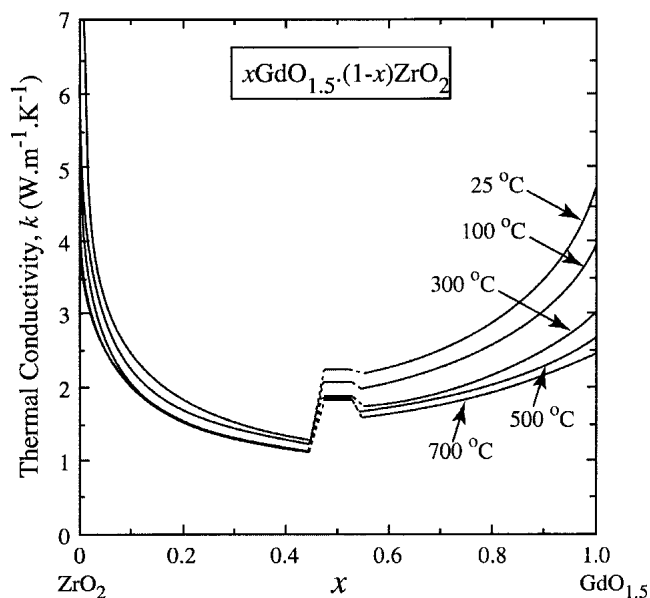


FIG. 3. Summary of theoretically calculated curves from Figs. 2(a)–2(e). Dashed lines are used to connect the curves and have no theoretical significance.

ZrO_2 and $\text{GdO}_{1.5}$. The measured thermal conductivity of pure ZrO_2 ^{16,17} was clearly found to be less dependent on the temperature than $1/T$ [Fig. 1(a)], and was found to approach a lower limit at elevated temperatures. This is possibly due to the limitation on the applicability of the intrinsic thermal conductivity theory to materials like ZrO_2 of short phonon mean free paths. This is also indicated by the small value of the empirical constant ($\chi = 0.51$) in Eq. (2). Furthermore, the smallest phonon mean free path, l_m (at the highest frequency, ω_M) at the highest measurement temperature ($T = 800$ °C) calculated using the intrinsic thermal conductivity theory [Eq. (4)] is about 4 Å. This value is smaller than the dimension $a_M (= a^3/N)^{1/3}$ of approximately 7 Å for ZrO_2 and is, therefore, physically unrealistic. The minimum phonon mean free path for $T_0 = 231$ K [Eq. (3)] is calculated [Eq. (4)] to be 19 Å, which is about three times the dimension a_M for ZrO_2 and is a more realistic value. In the case of pure $\text{GdO}_{1.5}$, the empirical constant in Eq. (1) ($\chi = 0.84$) is closer to unity than that in the case of ZrO_2 ($\chi = 0.51$), indicating better agreement between intrinsic thermal conductivity theory and the experimental data. The minimum thermal conductivity theory [Eq. (5)] was also fitted to the experimental data for pure $\text{GdO}_{1.5}$ with $T_0 = 235$ K. The corresponding minimum phonon mean free path is calculated [Eq. (4)] to be 22 Å, which for $\text{GdO}_{1.5}$ is also about four times the dimension $a_M = 6$ Å.

The semiempirical theory also describes the trends in the thermal conductivities of $x\text{GdO}_{1.5} \cdot (1-x)\text{ZrO}_2$ solid solutions as a function of composition (x) and temperature (T). On the ZrO_2 -rich side, the theory accurately captures the dramatic decrease in thermal conductivity with increasing x , for small values of x . Near-unity value for the empirical constant ($\psi = 1.06$) attests to the validity of this theory. For pyrochlore $\text{Gd}_2\text{Zr}_2\text{O}_7$ ($x = 0.5$), the theory adequately describes the temperature dependence of the thermal conductivity but only when the phonon-scattering contribution of oxygen vacancies is omitted. On the $\text{GdO}_{1.5}$ -rich side, the theory captures the composition and temperature dependence of thermal conductivity not as well ($\psi = 3.3$). Also, thermal conductivity values at $x = 0.89$ are higher than the trend at all temperatures. At that composition an ordered hexagonal phase is present, while the phases at all other intermediate compositions are cubic,²⁶ which is possibly responsible for this deviation.

Recently, Nicholls *et al.*²⁸ and Zhu and Miller²⁹ have used the concept of codoping of YSZ (4.6 mol% Y_2O_3) with one or more oxides (M_2O_3 ; $\text{M} = \text{Yb}, \text{Gd}, \text{Nd}, \text{Sm}, \text{Sc}$) to achieve lower thermal conductivities, which have been attributed to defect-cluster formation.²⁹ However, those measurements were made on porous coatings of unknown densities and, as such, cannot be readily compared with the fully dense thermal conductivities measured here.

VI. SUMMARY

The thermal conductivity of ceramics in the $\text{ZrO}_2\text{-GdO}_{1.5}$ system was measured as a function of temperature and composition. On the ZrO_2 -rich side, the thermal conductivity was found to decrease rapidly with increasing concentration of $\text{GdO}_{1.5}$ and was then found to reach a plateau. On the $\text{GdO}_{1.5}$ -rich side, that trend with increasing concentration of ZrO_2 was found to be less pronounced. The thermal conductivity of the solid solutions was found to become less sensitive to the composition with increasing temperature. The thermal conductivity of pyrochlore $\text{Gd}_2\text{Zr}_2\text{O}_7$ was found to be higher than the plateau values at all temperatures. A semiempirical phonon-scattering theory was used to analyze the experimental thermal conductivity data. In the case of pure ZrO_2 and $\text{GdO}_{1.5}$, the temperature dependence of the thermal conductivity was less pronounced relative to the $1/T$ temperature dependence. Therefore, the minimum thermal conductivity theory was applied, which captures better the temperature dependence of the thermal conductivity of pure ZrO_2 and $\text{GdO}_{1.5}$. In the case of solid solutions, the theory described the composition and temperature dependence of the thermal conductivity. For the ZrO_2 -rich side, Gd solute atoms and associated O vacancies were considered as the primary phonon-scattering point defects, whereas, for the Gd-rich side, Zr solute atoms and Gd vacancies were considered. In the case of $\text{Gd}_2\text{Zr}_2\text{O}_7$, only Gd solute atoms were considered.

ACKNOWLEDGMENTS

The authors thank Mr. B. Berke, Dr. T. Bhatia, and Mr. X. Wei for experimental assistance and discussions. The research at the University of Connecticut was supported by the United States Department of Energy/Advanced Gas Turbines Research (AGTSR) Grant No. 00-01-SR081 (administered by the South Carolina Institute of Energy Studies), and the research at the Instituto de Cerámica y Vidrio was supported by the Spanish Government under Grant Nos. MICYT (ES) MAT2000-767-C03-01 and CAM (ES) 07N/0030/2001.

REFERENCES

1. G. Suresh, G. Seenivasan, M.V. Krishnaiah, and P.S. Murti, *J. Nucl. Mater.* **249**, 259 (1997).
2. N.P. Padture, M. Gell, and E.H. Jordan, *Science* **296**, 280 (2002).
3. D.J.M. Bevan and E. Summerville, in *Handbook on the Physics and Chemistry of Rare Earths: Non-Metallic Compounds I*, edited by K.A. Gschneider and L.R. Eyring (North-Holland Physics Publishing, New York, 1979), Vol. 3, p. 412.
4. M.A. Subramanian and A.W. Sleight, in *Handbook on the Physics and Chemistry of Rare Earths*, edited by K.A. Gschneider and L. Eyring (Elsevier Science Publishers, Oxford, U.K., 1993), Vol. 16, p. 225.

5. R. Vaßen, X. Cao, F. Tietz, D. Basu, and D. Stöver, *J. Am. Ceram. Soc.* **83**, 2023 (2000).
6. M.J. Maloney, U.S. Patent No. 6 117 560 (2000).
7. M.J. Maloney, U.S. Patent No. 6 284 323 (2001).
8. G. Suresh, G. Seenivasan, M.V. Krishnaiah, and P.S. Murti, *J. Alloys Compd.* **269**, L9 (1998).
9. J. Wu, X. Wei, N.P. Padture, P.G. Klemens, M. Gell, E. Garcia, P. Miranzo, and M.I. Osendi, *J. Am. Ceram. Soc.* **85** (2002).
10. T.A. Ring, *Fundamentals of Ceramic Powder Processing and Synthesis* (Academic Publishers, New York, 1996).
11. K.D. Maglic, A. Cezairliyan, and V.E. Peletsky, *ASTM Standards E1461-92, E1269-92* (Plenum Press, New York, 1992).
12. O. Kubaschewski and C.B. Alcock, *Metallurgical Thermochemistry* (Pergamon Press, London, U.K., 1967).
13. R.A. Swalin, *Thermodynamics of Solids* (John Wiley & Sons, New York, 1972).
14. P.G. Klemens, *High Temp.-High Press.* **23**, 241 (1991).
15. K.W. Schlichting, N.P. Padture, and P.G. Klemens, *J. Mater. Sci.* **36**, 3003 (2001).
16. S. Raghavan, H. Wang, R.B. Dinwiddie, W.D. Porter, and M.J. Mayo, *Scr. Mater.* **39**, 1119 (1998).
17. S. Raghavan, H. Wang, W.D. Porter, R.B. Dinwiddie, and M.J. Mayo, *Acta Mater.* **49**, 169 (2001).
18. P.G. Klemens, in *Thermal Conductivity*, edited by R.P. Tye (Academic Press, London, U.K., 1969), Vol. 1, p. 1.
19. P.G. Klemens, in *Thermal Conductivity 23*, edited by K.E. Wilkes, R.B. Dinwiddie, and R.S. Graves (Technomics Publishing Co., Lancaster, PA, 1996), p. 209.
20. G.A. Slack, in *Solid State Physics*, edited by H. Ehrenreich, F. Seitz, and D. Turnbull (Academic Publishers, New York, 1979), Vol. 34, p. 1.
21. D.J. Green, R.H.J. Hannink, and M.V. Swain, *Transformation Toughening of Ceramics* (CRC Press, Boca Raton, FL, 1989).
22. D. Balestrieri, Y. Philipponneau, G.M. Decroix, Y. Jorand, and G. Fantozzi, *J. Eur. Ceram. Soc.* **18**, 1073 (1998).
23. M.C. Roufousse and P.G. Klemen, *J. Geophys. Res.* **79**, 703 (1974).
24. J. Tavernier, *C. R. Acad. Sci.* **245**, 1705 (1957).
25. C.A. Ratsifaritana and P.G. Klemens, *Int. J. Thermophys.* **8**, 737 (1987).
26. M. Perez-Y-Jorba, *Ann. Chim. (Paris)* **7**, 479 (1962).
27. J.H. Harris, R.C. Erk, and R.A. Youngblood, *Phys. Rev. B* **47**, 5428 (1993).
28. J.R. Nicholls, K.J. Lawson, A. Johnstone, and D.S. Rickerby, *Surf. Coat. Technol.* **151**, 383 (2002).
29. D. Zhu and R.A. Miller, *Ceram. Eng. Sci. Proc.* **23**, (2002, in press).